HHS Public Access

Author manuscript

J Mol Cell Cardiol. Author manuscript; available in PMC 2024 April 01.

Published in final edited form as:

J Mol Cell Cardiol. 2023 April ; 177: 28–37. doi:10.1016/j.yjmcc.2023.01.008.

Drp1/p53 interaction mediates p53 mitochondrial localization and dysfunction in septic cardiomyopathy

Riddhita Mukherjee, PhD[1,2,∓], **Laura H. Tetri, MD PhD**[1,3,∓], **Sin-Jin Li, PhD**[1], **Giovanni Fajardo, MD**[4], **Nicolai P. Ostberg, BS**[2], **Kaleb B. Tsegay, BS**[1], **Kanika Gera, PhD**[1], **Timothy T. Cornell, MD**[1], **Daniel Bernstein, MD**[4], **Daria Mochly-Rosen, PhD**[2], **Bereketeab Haileselassie, MD**[1,2]

[1]Department of Pediatrics, Division of Critical Care Medicine, Stanford University School of Medicine, Stanford, CA, 94305; USA

[2]Department of Chemical and Systems Biology, Stanford University School of Medicine, Stanford, CA, 94305; USA

[3]Department of Anesthesia, Perioperative and Pain Medicine, Stanford University School of Medicine, Stanford, CA, 94305; USA

[4]Department of Pediatrics, Division of Cardiology, Stanford University School of Medicine, Stanford, CA, 94305; USA

Abstract

Background: Previous studies have implicated p53-dependent mitochondrial dysfunction in sepsis induced end organ injury, including sepsis-induced myocardial dysfunction (SIMD). However, the mechanisms behind p53 localization to the mitochondria have not been well established. Dynamin-related protein 1 (Drp1), a mediator of mitochondrial fission, may play a role in p53 mitochondrial localization. Here we examined the role of Drp1/p53 interaction in SIMD using *in vitro* and murine models of sepsis.

Methods: H9c2 cardiomyoblasts and BALB/c mice were exposed to lipopolysaccharide (LPS) to model sepsis phenotype. Pharmacologic inhibitors of Drp1 activation (ΨDrp1) and of p53 mitochondrial binding (pifithrin μ, PFTμ) were utilized to assess interaction between Drp1 and p53, and the subsequent downstream impact on mitochondrial morphology and function, cardiomyocyte function, and sepsis phenotype.

Results: Both *in vitro* and murine models demonstrated an increase in physical Drp1/p53 interaction following LPS treatment, which was associated with increased p53 mitochondrial

[*]**Corresponding author:** Bereketeab Haileselassie MD MHS, Department of Pediatrics Division of Critical Care Medicine, Stanford University School of Medicine, Stanford, CA;, bhailes3@stanford.edu, Telephone number:650-497-7894.

[+]Shared first authorship

Authors' contributions: R.M, L.T, and B.H. contributed to manuscript preparation. R.M, and B.H generated the hypothesis. T.C, D.B and D.M-R aided with experimental design. R.M, B.H, G.F, N.P.O, K.B.T, K.G, L.T. conducted experiments and/or helped with data analysis. All the authors reviewed and edited the manuscript.

localization, and mitochondrial dysfunction. This Drp1/p53 interaction was inhibited by ΨDrp1, suggesting that this interaction is dependent on Drp1 activation. Treatment of H9c2 cells with either ΨDrp1 or PFTμ inhibited the LPS mediated localization of Drp1/p53 to the mitochondria, decreased oxidative stress, improved cellular respiration and ATP production. Similarly, treatment of BALB/c mice with either ΨDrp1 or PFTμ decreased LPS-mediated mitochondrial localization of p53, mitochondrial ROS in cardiac tissue, and subsequently improved cardiomyocyte contractile function and survival.

Conclusion: Drp1/p53 interaction and mitochondrial localization is a key prodrome to mitochondrial damage in SIMD and inhibiting this interaction may serve as a therapeutic target.

Keywords

mitochondrial fission; mitochondrial function; mitochondrial dynamics; septic cardiomyopathy; deltaPKC; bioenergetics; isolated cardiomyocyte; lipopolysaccharide; LPS sepsis model

Background:

Despite major clinical advances, sepsis continues to be a significant cause of global morbidity and mortality.[1,2] Out of the myriad of complications associated with sepsis, myocardial dysfunction has become increasingly recognized, with observational studies reporting incidence as high as 60%.[3,4] Furthermore, myocardial dysfunction in sepsis is an independent predictor of acute and long-term mortality.[5] Whereas the significance of cardiac failure in sepsis-associated mortality is well described, the pathobiology mediating cardiac dysfunction in sepsis remains unclear.[6]

Previous studies have demonstrated that p53, a key regulator of apoptosis, appears to mediate sepsis-induced end organ failure.[7] Excessive p53-dependent pro-apoptotic proteins have been found in end organs of patients suffering from sepsis induced multi-organ dysfunction syndrome (MODS)[8], leading to the development of clinical predictive models that use p53 signaling pathways to estimate morbidity and mortality in sepsis cohorts.[9] Despite these findings, previous attempts to induce global suppression of p53 in sepsis have shown limited efficacy in improving survival.[7] However, targeting specific functions of p53 has not been attempted. In particular, mitochondrial localization of p53 has been shown to play a significant role in mitochondrial dysfunction by post-translational modification of key regulatory proteins that are essential for mitochondrial dynamics, mitochondrial ROS clearance and mtDNA maintenance.[10-13] In addition, mitochondrial localization of p53 can increase mitochondrial oxidative stress and impair bioenergetics through the formation of mitochondrial permeability transition pore (MPTP).[14] Therefore, understanding the mechanisms that regulate mitochondrial localization of p53 might provide specific therapeutic targets for sepsis-induced end-organ failure, including myocardial dysfunction.

Recent literature has suggested that dynamin-related protein 1 (Drp1), a key mediator of mitochondrial fission, is essential for p53 mitochondrial localization and mitochondrial dysfunction in animal models of stroke and podocyte injury .[15,16] Drp1 is predominantly cytosolic, but upon activation, Drp1 is recruited to the mitochondrial surface where it binds to the mitochondrial adaptors including fission 1 (Fis1), mitochondrial fission factor

(Mff) and mitochondrial dynamics proteins 49 and 51 (Mid 49 and 51) to assemble the infrastructure required for mitochondrial fission.[17-19] Our group has demonstrated that Drp1 activation and Drp1/Fis1-dependent mitochondrial fission is a key driver to sepsis-induced mitochondrial dysfunction and myocardial failure in our murine models.[20-22] However, the mechanistic role of Drp1/p53 interaction on p53 mitochondrial localization and subsequent p53-dependent mitochondrial dysfunction has not been explored in sepsis. Using previously validated inhibitors of Drp1 activation (ΨDrp1) and p53 mitochondrial binding (PFTμ), we examined the impact of Drp1/p53 interaction on cardiomyocytes' mitochondria and on their contractile function in models of septic cardiomyopathy.[23]

Materials and Methods

Peptide and small molecule inhibitors

Drp1/ δPKC interaction inhibitor, peptide ΨDrp1 ((YTDFDE-GG-YGRKKRRQRRR) and vehicle peptide TAT (derived from TAT47-57; YGRKKRRQRRR) described before[23], were synthesized by Ontores Biotechnologies (Hangzhou, China) and dissolved in ultrapure PBS. The purity of peptides was > 90%, as determined by RP-HPLC. Pifithrin-μ (PFTμ), a small molecule which inhibits p53-mitochondria interaction, was obtained from MedChemExpress (#HY-10940) and dissolved in 10% anhydrous DMSO.[24]

Cell lines and *in vitro* treatment groups

H9c2 cardiomyocytes were cultured in DMEM supplemented with 10% FBS and 4 mM glutamine in 10 cm petri dishes and grown in a 5% CO_2 atmosphere at 37°C. H9c2 cardiomyocytes were seeded and allowed to attach before being treated with LPS (Sigma Cat# L4391) in DMEM containing 0.5% FBS. While doses of LPS ranged between 1 – 10 μg/ml in different *in vitro* experiments, treatment during each experiment were the same across all treatment groups. Treatment of H9c2 cells with 2 μM ΨDrp1 peptide or 5 μM PFTμ small molecule was carried out in DMEM without FBS.

Plasmid vector modification and transfection

H9c2 cells were seeded at a density of 50,000 cells/well in 12-well plates with DMEM containing 10% FBS media. The following day, cells were transfected with 1.6 μg of mCh-Drp1^{WT} or mCh-Drp1^{S616E} plasmids,[25] using 4 μl Lipofectamine2000 (Thermo Fisher Scientific) volume/well in serum-free media. Media was changed to DMEM containing 10% FBS media 5–6 hours after siRNA transfection and mCh fluorescence was evaluated at 24, 48 and 72 hrs post transfection to identify optimal transfection efficiency. After identifying optimal time, cells were evaluated for Drp1 phosphorylation at S616 as well as Drp1 and p53 mitochondrial localization by western blot, as described below.

Animals and *in vivo* treatment groups

All animal experiments were carried out under the protocols (#33002) approved by the Institutional Animal Care and Use Committee of Stanford University. For tissue analysis, 7-week-old BALB/c mice were randomized into vehicle control, LPS, LPS + ΨDrp1 and LPS + PFTμ model of sepsis groups. LPS at 8 mg/kg (dissolved in 0.2 ml of saline), ΨDrp1at 0.5mg/kg (dissolved in 0.2 ml of saline) and PFTμ at 25 mg/kg (dissolved in

0.2 ml, 9:1 v/v in corn oil) were administered intraperitoneally. Animals were sacrificed 1 hour and 24 hours post LPS-dosing and cardiac tissue was collected to evaluate Drp1-p53 interaction, mitochondrial localization as well as oxidative stress, as described below.

For isolated cardiomyocyte analysis, illness severity, and mortality, 7-week-old Balb/c mice were randomized into vehicle control, LPS (13mg/kg), LPS + ΨDrp1(0.5mg/kg) and LPS + PFTμ (25mg/kg) groups. Previously validated mouse sepsis scoring tool was used to assess illness severity, as described.[26] To address the batch to batch variability of LPS potency, dose for cardiac function and mortality analysis was chosen based on dose titration experiments using the available aliquot from manufacturer to attain a mortality rate of 50-60% at 48 hrs. post injection. The same batch of LPS was used for all biological replicates.

Echocardiogram Analysis

Balb/c mice underwent echocardiogram at baseline and at 18 hours post treatment with vehicle, LPS, LPS + ΨDrp1, or LPS + PFTμ to attain velocity time integral (VTI) across the left ventricular outflow tract (LVOT). Transthoracic echocardiography was performed using the Vivid e95 platform (GE Medical Systems, Milwaukee, WI, USA). Two-dimensional, M-mode, and doppler echocardiographic examinations were performed using a L8-18i linear transducer. Two-dimensional imaging was acquired at a minimum depth setting of 2 cm and the images were adjusted to the heart size with the enhanced resolution imaging function. All M- mode and doppler spectra are recorded at a sweep speed of 200 mm/s for off-line analysis. For each mouse, between 9 and 13 heartbeats were used to measure VTI and maximum velocity, which were then averaged. Images were analyzed by a scientist blinded to condition groups.

Isolated Cardiomyocytes

Myocyte isolation—Ventricular myocytes were isolated from BALB/c mice 18 hours after treatment with vehicle, LPS, LPS + ΨDrp1, or LPS + PFTμ, based on previously published protocols with modifications.[27,28] Mice were injected with heparin (100 IU/ml) and anesthetized with pentobarbital sodium (100 mg/kg intraperitoneal). The heart was removed and retrogradely perfused at 37°C with a calcium free solution (120mM NaCl, 14.7mM KCl, 0.6mM KH_2PO_4, 0.6mM Na_2HPO_4, 1.2mM $MgSO_4$-$7H_2O$, 4.6mM $NaHCO_3$, 10mM Na-HEPES, 30mM taurine, 10mM BDM, 5.5mM glucose) for 4 min followed by an enzymatic digestion with collagenase (Worthington Biochemical Corporation, Lakewood, NJ; 394U/mg, 1.5 mg/ml). The digestion was initially performed in calcium free solution for 2 min and then $CaCl_2$ was added to 50 μM final concentration for 6 additional minutes. Ventricles were dissected into small pieces and were further digested by gently disruption with plastic transfer pipettes for 3-5 min. ‘Stop buffer’ (calcium free solution with $CaCl_2$ 12.5 μM and 10% bovine calf serum (Hyclone, Logan, UT)) was added and cell suspension was centrifuged at 350 rpm for 3 min. Myocytes were resuspended in stop buffer containing 100 μM $CaCl_2$, rested for 3 min and then centrifuged at 350 rpm for 3 min. These steps were repeated using stop buffer with increasing $CaCl_2$ concentrations until 1mM was achieved. Experiments were performed with freshly isolated myocytes resuspended

in a HEPES-buffered solution (1mM $CaCl_2$, 137mM NaCl, 5.4mM KCl, 15mM dextrose, 1.3mM $MgSO_4$, 1.2mM NaH_2PO_4, 20mM HEPES, pH 7.4).

Ex Vivo Myocyte Contractility and Calcium Transient:

Cell contraction properties of myocytes were evaluated with a video-based sarcomere spacing acquisition system (SarcLen, IonOptix, Milton, MA). Rod-shaped myocytes with clear striation patterns and quiescent when unstimulated were chosen. For calcium flux measurements, myocytes were loaded with 0.5 mM fura 2-acetoxymethyl ester (Molecular Probes, Eugene, Oregon, USA) for 15 min. Cells were then washed and rested for an additional 40 min to allow the de-esterification of the fura-2 ester. Cells were placed in a culture chamber stimulation system (Cell MicroControls, Norfolk, VA), mounted on an inverted microscope (Nikon TE2000U, Nikon, Melville, NY) and electrically stimulated with suprathreshold voltage at 0.5 Hz and superfused with a HEPES-buffered solution at 25°C as previously described.[29,30] Changes in sarcomere length were recorded and further analysis was performed using IonWizard software (IonOptix, Milton, MA). Cells were excited at 340 and 380 nm, continuously alternated, at rates as high as 250 pairs/sec using a HyperSwitch system (IonOptix, Milton, MA). Background-corrected fura-2AM ratios were collected at 510 nm. This ratio is independent of cell geometry and excitation light intensity, and reflected the intracellular calcium concentration.[31,32]

Analysis of mitochondrial morphology

H9c2 cells cultured on 96 well chamber were incubated with different treatment conditions (LPS and LPS + ΨDrp1 or PFTμ). Following treatment, cells were incubated with 66 nM Mitotracker Deep Red (cat# M22426, Invitrogen, CA) and DAPI (1:10,000) for 20 minutes and images were acquired using an All-in-One Fluorescence Microscope BZ-X700 (Keyence). Mitochondrial morphology in H9c2 cardiomyocytes was analyzed using a macro in ImageJ to assess mitochondrial interconnectivity and length from fluorescence micrographs, according to previously published protocol.[33] Major axis length was defined as the length of the longest line that can be drawn through a binary object, whereas the minor axis length was defined as the length of the shortest line. The aspect ratio was defined by the major axis length divided by the minor axis length.

Mitochondrial membrane potential

H9c2 cardiomyocytes were incubated with 20 nM tetra-methyl-rhodamine methyl ester (TMRM) (Invitrogen, CA) and DAPI (1:10,000) in HBSS (Hank's balanced salt solution) for 20 min at 37°C, as per the manufacturer's protocol. The fluorescence was analyzed on a SpectraMax M2e microplate reader (Molecular devices, CA) at excitation/emission maxima of 544/645 nm for TMRM and 350/470 nm for DAPI. All data were normalized to (a) the number of cells per well, as quantified by total number of DAPI+ nuclei, and to (b) the TMRM fluorescence intensity of the controls.

Mitochondrial ROS production

For detection of mitochondrial ROS production, cells were treated for 20 min with 5 μM MitoSOX™ Red, a mitochondrial superoxide indicator (Invitrogen, CA), along with DAPI at

37°C in the dark, according to the manufacturer's protocol, and fluorescence was analyzed using SpectraMax M2e microplate reader (Molecular devices, CA) at excitation/emission maxima of 510/588 nm.

ATP measurements

Adenosine triphosphate level in H9c2 cells was assayed by the ATP detection luminescence assay kit (Cayman Chemical, Cat#700410) per manufacturer's protocols. H9c2 cells were lysed in 0.05% Triton-X lysis buffer, incubated at 95°C for 7 minutes and centrifuged to collect the protein lysate. Total protein concentration was quantified using bicinchoninic acid assay (BCA) protein. Three technical replicates were conducted from each sample. Luminescent signal, proportional to ATP level was measured using SpectraMax M2e microplate reader (Molecular devices, CA) and was normalized to total protein concentration of H9C2 cells.

Bioenergetic profile

H9c2 cells were plated at 18,000 cells per well on Seahorse XFe24 Cell Culture Microplate (Agilent, Cat#101085-004, Santa Clara, CA) and treated with LPS (1 μg/ml), ΨDrp1 (1μM) and/or PFTμ (5 μM) for 24 hours. At the end of the experiment, cells were washed twice with Agilent Seahorse XF Media, supplemented with 1 mM pyruvate, 2 mM L-glutamine, and 2 mM D-glucose; a final volume of 525 μl was placed in each well. Cells were then incubated in a 0% CO2 chamber at 37°C for 1 h before analysis on a Seahorse XFe24 Analyzer (Agilent, Santa Clara, CA). MitoStress assays were performed by treating the cells sequentially with 1 μM oligomycin, 2 μM carbonyl cyanide p-trifluoromethoxy phenylhydrazone (FCCP), and 0.5 μM rotenone/antimycin. A total of three oxygen consumption rate (OCR) and extracellular acidification rates (ECAR) measurements were taken after each compound was administered. Metabolic balance between aerobic and anerobic metabolism was assessed averaged over each compound as a ratio of OCR/ECAR.

Isolation of mitochondria-enriched fraction and lysate preparation

H9c2 cells were scraped off their plates in DMEM, washed once with cold phosphate-buffered saline (PBS) and resuspended in mannitol–sucrose (MS) buffer, containing 210 mM mannitol, 70 mM sucrose, 5 mM MOPS (3-(N-morpholino) propane-sulfonic acid), 1 mM EDTA, and a protease inhibitor cocktail, pH 7.4. The cells were then disrupted by repeated aspiration through a 27-1/2-gauge needle. Cardiac tissue was diced into small pieces using a scalpel and homogenized in MS buffer added with protease-inhibitor cocktail on ice using a Dounce homogenizer. The homogenates were then centrifuged at 800 g for 15 min at 4°C to extract the nuclear pellet. The resulting supernatants were aliquoted and used as total lysates. A second aliquot was centrifuged at 20,000 g for 30 min at 4°C. The pellets were surface-washed with MS buffer and extracted as mitochondrial-rich fractions by resuspending in MS buffer containing 0.1% Triton X-100 and protease inhibitor cocktail.[34,35]

Co-immunoprecipitation assay

Total protein concentrations of cell or cardiac tissue lysates were determined using the BCA assay (Thermo Scientific Cat#23227, Hercules, CA). Drp1 and its interacting proteins

were immunoprecipitated using an anti-Drp1 mouse monoclonal antibody (BD Transduction Laboratories; 611113). Mouse IgG was used as a negative control. The antibodies were crosslinked to magnetic beads (Pierce Protein A/G Magnetic beads › Cat #: 88802), to ensure heavy chain IgG removal from the final protein extract. Briefly, the magnetic beads were incubated with anti-Drp1 antibody or IgG only at room temperature for 2 hours with rotation, followed by washing in conjugation buffer (20 mM Na phosphate, 0.15 M NaCl, pH 7-9) and crosslinking with 5 mM BS3 after which the crosslinking reaction was quenched by 1M Tris HCl (pH 7.5). The antibody-bead conjugates were then incubated with protein lysate from each treatment condition. Finally, the lysates were washed in lysis buffer (1% Triton-X in 1X PBS and 1X protease inhibitor cocktail) and eluted in Laemmli buffer containing 2-mercaptoethanol. The immunoprecipitates were chromatographed on a SDS-PAGE and immunoblotted with anti-Drp1 rabbit monoclonal antibody (Cell Signaling Technology; 8570; 1:1000, Danvers, MA) and anti-p53 rabbit polyclonal antibody (Abcam; ab131442; 1:500, Burlingame, CA). 15 μl total input proteins as well as IgG negative controls were included for all treatment conditions. Non-heavy-chain specific anti-rabbit (Cat#ab99697) and anti-mouse (Cat#ab131368) secondary antibodies were obtained from Abcam (Danvers, MA).

Western blot analysis

Protein concentrations of cell or tissue lysates were determined using the BCA assay (Thermo Scientific Cat # 23227, Hercules, CA). Proteins were resuspended in Laemmli buffer containing 2-mercaptoethanol, loaded on SDS–PAGE, and transferred on to 0.45 μm nitrocellulose membrane, as described before (Biorad Cat#1704270, Hercules, CA). Membranes were probed with the indicated antibody and then visualized by enhanced chemiluminesence substrate (Biorad Cat # 170506S, Hercules, CA). Images acquired with Biorad Chemidoc Imager (Hercules, CA) were analyzed with ImageJ to determine relative band intensity. Quantification was performed on samples from independent cell cultures or animal tissue lysates for each treatment condition. The antibodies used in this study were: Anti-β-actin (8H10D10) mouse monoclonal antibody (Cell Signaling Technology; 3700; 1:1000, Danvers, MA); Anti-VDAC1 (20B12AF2) mouse monoclonal antibody (Abcam; 14734; 1:500, Burlingame, CA); Anti-Drp1 (Clone 8/ DLP1 (RUO)) mouse monoclonal antibody (BD Transduction Laboratories; 611113; 1:100, San Jose, CA); Anti-phospho-Drp1 (Ser616) rabbit polyclonal antibody (Cell Signaling Technology; 3455; 1:250, Danvers, MA); Anti-p53 mouse monoclonal antibody (Santa Cruz; sc-126; 1:250, Dallas, TX). Secondary antibodies including anti-mouse IgG (Cat#NA931V) and anti-rabbit IgG (Cat#NA934V) were obtained from GE Healthcare (Chicago, IL). Detailed antibody validation profiles are available from aforementioned source companies.

In situ proximity ligation assay (PLA)

Drp1/p53 protein/protein interactions in H9c2 cells under various treatment conditions was visualized in situ using the Duolink PLA Fluorescence Kit (Sigma-Aldrich, Cat#DUO92101, St Louis, MO). Briefly, H9c2 cells, seeded and treated in chamber slides, were fixed in 4% paraformaldehyde and permeabilized in 0.2% PBS-Tx. Cells were blocked in Blocking Solution incubated with primary antibodies diluted in Duolink Antibody Diluent. The primary antibodies used were: anti-Drp1 mouse monoclonal antibody (BD

Transduction Laboratories; 611113; 1:50, San Jose, CA) and anti-p53 rabbit polyclonal antibody (Abcam; ab131442; 1:100, Burlingame, CA). Following washing in wash buffer A, cells were incubated with secondary antibodies conjugated with PLUS (anti-rabbit PLUS) and MINUS (anti-mouse MINUS) probes for one hour at 37°C. The cells were then washed and incubated with the ligase (diluted 1:40 in ligation buffer) following which cells were incubated with the polymerase (diluted 1:80 in an amplification buffer) for the signal amplification cycle. Finally, the cells were washed in wash buffer B and mounted in antifade fluorescence mounting medium containing DAPI (Vectashield). All images were acquired using an All-in-One Fluorescence Microscope BZ-X700 at 20X and 40X magnification. Following image acquisition, volocity acquisition software (Quorum Technologies inc. Puslinch, ON) was used to draw regions of interest (ROI) around randomly selected cells across different conditions. Volocity software was subsequently used to quantify the number of fluorescent puncta in each ROI above a specified signal threshold. Image analysis was performed by a scientist who was blinded to the experimental groups.

Dihydroethidium (DHE) staining

ROS levels were detected in frozen heart sections by dihydroethidium (DHE) fluorescence staining. Briefly, slides with 10 μm OCT-frozen transverse heart sections were washed in ultrapure water and then incubated in opaque coplin jars containing 5 μM DHE solution. Afterwards, slides were rinsed twice with ultrapure water and mounted in antifade fluorescence mounting medium containing DAPI (Vectashield). Images were acquired immediately using an All-in-One Fluorescence Microscope BZ-X700 at 20X and 40X magnification. Cardiac sections from 3 animals of each treatment condition were used for imaging and analysis.

Detection of S-nitrosylated proteins in heart mitochondrial lysates

Detection of ROS-induced formation of S-nitrosylated proteins in mitochondrial pellets from mouse heart was carried according to manufacturer's protocol (Pierce S-Nitrosylation Western blot kit, Thermo Scientific, MA). Briefly, all protein samples (adjusted to starting concentration of 2mg/ml to 100μl volume in HENS buffer) were first treated with a sulfhydryl-reactive compound, MMTS, that blocked all unmodified cysteines. Then the remaining S-nitrosylated cysteins were reduced a sodium ascorbate (or not reduced, as a negative control to the experiment) and subsequently labeled with iodo-TMT reagent. Finally, the total lysate was run on Western blot and the iodo-TMT labeled (i.e., S-nitrosylated) proteins were detected by an anti-TMT antibody (1:1000, Thermo Scientific). Each sample was normalized to total protein level as detected by Ponceau staining.

Statistical analyses

Construction of graphs and calculations of statistical significance were performed using Prism 9.0 (Graphpad). The presented quantified experiments were evaluated based on the average of three or more independent experiments and calculated as mean values ± SD. Normally distributed variables with 3 or greater conditions were compared by ANOVA. Non-normally distributed variables were evaluated using Mann-Whitney U-test for pairwise comparisons and Kruskal-Wallis for multiple comparison. The nominal p value of <.05 was used as statistically significant threshold.

Results:

Mitochondrial localization of p53 is dependent on Drp1 activation and direct p53 and Drp1 interaction.

To determine the relationship between Drp1 activation and p53 mitochondrial localization in the *in vitro* septic cardiomyopathy model, we first evaluated the association between Drp1 and p53 mitochondrial localization following LPS treatment. LPS induced an early increase in mitochondrial localization of p53, which temporally correlated with Drp1 mitochondrial localization following LPS treatment (Figure 1A). To demonstrate that p53 mitochondrial localization is directly associated with Drp1 activation independent of LPS, we expressed a wildtype (mCh-Drp1^{wt}) and phosphomimetic Drp1 mutant (mCh-Drp1^{S616E}) in the H9c2 cardiomyocytes and evaluated changes in p53 mitochondrial localization patterns. When compared to wildtype, H9c2 cells that were transfected with phosphomimetic Drp1 mutant (mCh-Drp1^{S616E}) had a significant increase in mitochondrial localization of p53 (Figure S1A) and resulted in subsequent reduced mitochondrial membrane potential and increased mitochondrial oxidative stress (Figure S1B-C). Together, these data suggest that LPS-mediated activation of Drp1 plays a role in p53 localization to the mitochondria.

To further assess whether Drp1 activation is essential for p53 mitochondrial localization upon LPS treatment, H9c2 cells were co-treated with LPS and ΨDrp1, a peptide inhibitor of δPKC-dependent Drp1 phosphorylation and activation (Figure S2A). Inhibition of Drp1 activation with ΨDrp1 resulted in a 4-fold reduction of p53 mitochondrial localization following LPS treatment (Figure 1A). To elucidate if this effect was driven by the physical interaction of activated Drp1 with p53, LPS-treated H9c2 cells with and without ΨDrp1 treatment were analyzed by co-immunoprecipitation assay and proximity ligation assay. Both assays revealed significantly increased Drp1/p53 binding following LPS treatment that was attenuated by ΨDrp1 (Figure 1B-C), suggesting that, following septic cues, p53 mitochondrial localization is, in part, mediated by direct Drp1/p53 interaction.

Inhibition of Drp1/p53 interaction and mitochondrial localization attenuates mitochondrial dysfunction in cell culture model of sepsis-induced cardiomyopathy.

Whereas mitochondrial networks are constantly in flux between fission and fusion, excess mitochondrial fission results in decreased metabolic function and increased oxidative stress.[18] Examination of the mitochondrial morphology in H9c2 cardiomyoblasts showed that LPS treatment altered the integrity of the mitochondrial network leading to excessive fragmentation. This phenotype significantly improved with ΨDrp1 treatment, which inhibits Drp1 activation, a key mediator of mitochondrial fission (Figure 2A&B). To determine if p53 mitochondrial localization contributes to the alterations in mitochondrial morphology following LPS treatment, we utilized PFTμ, a small molecule inhibitor which interrupts p53 – mitochondria interaction (Figure S3).[24] Co-treatment with LPS and PFTμ significantly reduced mitochondrial fragmentation when compared to LPS alone (Figure 2A&B).

The alterations in mitochondrial morphology following LPS treatment coincided with a significant decrease in mitochondrial membrane potential (Figure 2C), increased mitochondria-specific oxidative stress (Figure 2D) as well as bioenergetic failure with

increased reliance on anaerobic metabolism (Figure 2F - I) resulting in a decrease in ATP production (Figure 2E). Treatment with both ΨDrp1, which inhibits Drp1 activation and thus Drp1/p53 interaction, and PFTμ, which interferes with p53 binding to the mitochondria, attenuated these detrimental effects of LPS (Figure 2C-I).

To determine if the impact of ΨDrp1 and PFTμ on the mitochondria are interdependent, we transfected Drp1 phosphomimetic (S616E) mutant into H9c2 cells which were subsequently treated with both ΨDrp1 and PFTμ. ΨDrp1 had minimal effect on mitochondrial oxidative stress when compared to phosphomimetic (S616E) mutant controls. However, PFTμ treatment significantly improved mitochondrial ROS in cells that were transfected with Drp1 phosphomimetic (S616E) mutant. This observation, that mitochondrial damage induced by constitutively active Drp1 can be partially mitigated by preventing p53 binding at the mitochondrial membrane suggests that p53 is necessary for at least one pathway through which Drp1 induces mitochondrial stress (Figure S4). Altogether, these results suggest a direct link between Drp1/p53 interaction, mitochondrial localization, and the mitochondrial dysfunction in the cell line model of septic cardiomyopathy.

Pharmacological inhibition of Drp1 activation and p53 mitochondrial localization limits mitochondrial damage and improves cardiac function in LPS mouse model of sepsis.

To evaluate the role of Drp1/p53 interaction in sepsis-mediated mitochondrial damage *in vivo*, we injected 7-week-old Balb/c mice with LPS (8mg/kg) intraperitonially. A subset of the LPS-treated mice was administered either with PFTμ (25mg/kg), to directly inhibit p53 mitochondrial localization, or with ΨDrp1 (0.5mg/kg), to inhibit Drp1 S616 phosphorylation and activation (Figure S5A). Similar to the in vitro findings (Figure 1C), inhibition of Drp1 activation with ΨDrp1 reduced Drp1/p53 binding in cardiac tissue of LPS-treated mice (Figure 3A). Furthermore, both PFTμ and ΨDrp1 significantly decreased the LPS-mediated p53 and Drp1 mitochondrial localization within an hour of LPS administration, represented by a decrease in p53 and Drp1 content in mitochondrial enriched fractions from cardiac tissue (Figure 3B). Decreasing mitochondrial localization of p53 using either PFTμ or ΨDrp1 attenuated LPS-mediated increase in oxidative stress in the mitochondria, as represented by oxidative post-translational modification (protein S-nitrosylation) of mitochondrial proteins from cardiac tissue (Figure 3C), as well as, in the overall oxidative stress in the cardiac tissue, as represented by dihydroethidium (DHE) staining (Figure 3D).

Previous studies have demonstrated that mitochondria play a substantial role in modulating the amplitude and timing of intracellular calcium flux by shifts in mitochondrial calcium buffering capacity as well as through close contact between mitochondria and endoplasmic reticulum (ER).[36-40] Therefore, the impact of LPS and inhibitors on calcium flux and contractility under electrical stimulation in isolated cardiomyocytes of the treated mice were assessed. LPS treatment significantly reduced baseline calcium, calcium efflux from the sarcoplasmic reticulum, peak calcium concentration, and sequestration rate (Figure 4A-D). Co-treatment with ΨDrp1 significantly improved baseline calcium concentration and resequestration rate while treatment with PFTμ significantly improved the calcium flux associated with contractility (Figure 4A, C & D). Importantly, LPS treatment significantly

reduced the rate of contraction, peak contraction, and rate of relaxation and these measures were attenuated by co-treatment with both ΨDrp1 and PFTμ (Figure 4E-G). To determine the functional cardiac effects of interrupting the Drp1/p53 interaction after treatment with LPS and inhibitors In vivo, maximum velocity and velocity time integral (VTI) across the aorta of the treated mice were assessed by echocardiography. LPS treatment significantly reduced both maximum velocity and VTI across the LVOT, a surrogate for stroke volume, while treatment with both ΨDrp1 and PFTμ reduced the effect of LPS on VTI (Figure 5A-B).

To determine the impact of inhibiting Drp1/p53 interaction on LPS-mediated disease severity, animals treated with LPS (13mg/kg) with or without inhibitors [PFTμ (25mg/kg) or ΨDrp1(0.5mg/kg)] were assessed for severity of illness using mouse sepsis scoring and mortality.[26] When compared to control, LPS significantly increased illness severity represented by decreased weight and increase in mouse sepsis score post LPS treatment. While, there was no significant differences in illness severity in the different septic groups these results are confounded by survival bias (Figure S6A-B). When looking at mortality, LPS-treated mice had a significant increase in mortality (0% *vs.* 64%; $p<0.0001$, for control *vs.* LPS), which was partially attenuated by interruption of the Drp1/p53 interaction with ΨDrp1 (64% *vs.* 40%; $p=0.044$, for LPS *vs.* LPS+ ΨDrp1) and PFTμ treatment (64% *vs.* 32%; $p=0.023$, for LPS *vs.* LPS+ PFTμ) (Figure 5C).

Discussion

Previous studies have implicated p53 activation and associated signaling in the development of sepsis induced multi-organ dysfunction syndrome (MODS).[7,32,34] However, due to the important role of p53 on a variety of cellular functions including transcriptional regulation, cell cycle and DNA damage repair, it is not surprising that global inhibition has not shown benefit in pre-clinical studies.[9] However, direct p53 mitochondrial localization, independent of its function at the nucleus, has been shown to contribute to mitochondrial dysfunction and subsequent cell death.[42] Therefore, the mechanisms which govern p53 mitochondrial localization could serve as a potential therapeutic target in SIMD. In this study, we used both PFTμ, a small molecule inhibitor of p53 binding at the mitochondrial surface, and ΨDrp1, a peptide inhibitor of Drp1 activation, in sepsis models to demonstrate that Drp1 activation plays a significant role in p53 stabilization and localization to the mitochondrial membrane. Furthermore, we demonstrated that interruption of this interaction prevents mitochondrial dysfunction, improves cardiomyocyte contractile function and decreases LPS-mediated mortality.

Drp1 is well known as a mediator of mitochondrial fission, which is essential for a variety of cellular functions including mitochondrial quality control and cell division.[7-9] However, excessive mitochondrial fragmentation, mediated through the Drp1/Fis1 interaction, has been shown to induce oxidative stress in a variety of disease models, including ischemia/reperfusion and neurodegenerative diseases.[17-19,21,34,43] In sepsis models, we have previously shown that selective inhibition of Drp1/Fis1 interaction reduces pathological mitochondrial fission and improves cellular respiration in metabolically active end-organs.[19,21] However, there are limited data on the role of Drp1 in mediating p53

dependent mitochondrial damage. Two previous studies described the interaction between Drp1 and p53 contributes to mitochondrial damage in pre-clinical models of stroke and renal failure.[15,16] Using pharmacological tools, our data highlights the significance of this mechanism in sepsis.

Using immunoprecipitation and proximity ligation assays, our results demonstrate that Drp1 mediated p53 mitochondrial localization is *via* direct protein-protein interaction. Previous mutagenesis studies have demonstrated that the interaction site likely sits in the GTPase domain of Drp1 and DNA binding domain of p53.[16] However, the manner by which these two proteins interact is still currently unknown. While our results demonstrate that blocking Drp1 activation decreases Drp1-p53 interaction and improves mitochondrial dysfunction, which indirectly suggests that this interaction indeed mediates LPS-induced mitochondrial dysfunction, future detailed characterization of this interaction site is necessary for development of therapeutics to modulate this mechanism.

While p53 is associated with worse outcomes in sepsis [7,32,34], the role of p53 has not been well delineated in SIMD. SIMD is associated with both systolic and diastolic dysfunction as well as mortality.[3,6,44] Here, we demonstrated both systolic and diastolic dysfunction in murine sepsis model, as measured by aortic VTI, isolated cardiomyocyte rate of contraction and relaxation, as well as calcium flux. Significant recovery of this contractile function with both interruption of Drp1/p53 interaction and inhibition of p53 mitochondrial-binding indicates that this cellular event plays a key role in SIMD. Despite improvement of contractile function, recovery of calcium flux was not clearly observed following co-treatment with pharmacologic inhibitors; which suggests that mechanisms other than calcium handling play an important role in the recovery of cardiac function. This observation is a notable finding as the mitochondria play a substantial role in calcium flux by direct calcium buffering[36-38] as well as through mitochondria-sarcoplasmic reticulum (SR) interactions.[39,40,45] It is likely that LPS mediated impact on SR function can be independent of mitochondria and therefore would not be recovered by limiting Drp1/p53 mediated mitochondrial damage. The improvement in myocardial contractility is likely due to increased efficiency in cellular respiration (Figure 2E-I) and limiting mitochondrial oxidative stress (Figure 2D & 2C-D), which impacts contractile function independent of calcium flux.[46-48]This apparent uncoupling of calcium flux and contractility requires further investigation on the effects of LPS on SR mediated calcium handling.

Finally, interruption of Drp1/p53 interaction and p53 association with the mitochondria had reduced mortality in this model. Despite survival benefit, inhibiting Drp1/p53 interaction was not associated with changes in sepsis scoring or weight loss. This is likely due to confounding by survival bias as the score only represents surviving animals within each group.

While Drp1 and p53 interaction has demonstrated mechanistic significance in our pre-clinical sepsis model, this interaction and its importance in the pathophysiology of SIMD have yet to be characterized in human sepsis. Recently published observational studies demonstrating increased p53 in the cardiac tissue of septic patients provides promising evidence,[8] however, further characterization of this pathway in sepsis biology

and the resultant phenotype is required for therapeutic development. Altogether, our findings highlight a role for Drp1, the mediator of mitochondrial fission, in p53-induced mitochondrial dysfunction, and suggest a possible therapeutic target for sepsis-induced myocardial dysfunction.

Supplementary Material

Refer to Web version on PubMed Central for supplementary material.

Acknowledgements:

This work was supported by NICHD R00 HD099387, and Maternal Child Research Institute MCHRI pilot grant to BH.

References:

1. Rubens M et al. Increasing Sepsis Rates in the United States: Results From National Inpatient Sample, 2005 to 2014. J. Intensive Care Med 35, 858–868 (2020). [PubMed: 30175649]
2. Rudd KE et al. Global, regional, and national sepsis incidence and mortality, 1990–2017: analysis for the Global Burden of Disease Study. The Lancet 395, 200–211 (2020).
3. Parker MM Profound but Reversible Myocardial Depression in Patients with Septic Shock. Ann. Intern. Med 100, 483 (1984). [PubMed: 6703540]
4. Beesley SJ et al. Septic Cardiomyopathy: Crit. Care Med 46, 625–634 (2018). [PubMed: 29227368]
5. Sanfilippo F et al. Left ventricular systolic function evaluated by strain echocardiography and relationship with mortality in patients with severe sepsis or septic shock: a systematic review and meta-analysis. Crit. Care 22, 183 (2018). [PubMed: 30075792]
6. Antonucci E et al. Myocardial depression in sepsis: From pathogenesis to clinical manifestations and treatment. J. Crit. Care 29, 500–511 (2014). [PubMed: 24794044]
7. Hotchkiss RS et al. p53-Dependent and -Independent Pathways of Apoptotic Cell Death in Sepsis. J. Immunol 164, 3675–3680 (2000). [PubMed: 10725725]
8. Reil PM et al. The Role of BCL2 Protein and Tumour Protein p53 in Septic Cardiomyopathy. 4.
9. Wong HR et al. Improved Risk Stratification in Pediatric Septic Shock Using Both Protein and mRNA Biomarkers. PERSEVERE-XP. Am. J. Respir. Crit. Care Med 196, 494–501 (2017). [PubMed: 28324661]
10. Matoba S et al. p53 Regulates Mitochondrial Respiration. Science 312, 1650–1653 (2006). [PubMed: 16728594]
11. Park J-Y et al. p53 Improves Aerobic Exercise Capacity and Augments Skeletal Muscle Mitochondrial DNA Content. Circ. Res 105, 705–712 (2009). [PubMed: 19696408]
12. Achanta G et al. Novel role of p53 in maintaining mitochondrial genetic stability through interaction with DNA Pol γ. EMBO J 24, 3482–3492 (2005). [PubMed: 16163384]
13. Saleem A & Hood DA Acute exercise induces tumour suppressor protein p53 translocation to the mitochondria and promotes a p53-Tfam-mitochondrial DNA complex in skeletal muscle: Exercise and mitochondrial p53. J. Physiol 591, 3625–3636 (2013). [PubMed: 23690562]
14. Dai C-Q et al. p53 and mitochondrial dysfunction: novel insight of neurodegenerative diseases. J. Bioenerg. Biomembr 48, 337–347 (2016). [PubMed: 27422544]
15. Yuan Y et al. p53/Drp1-dependent mitochondrial fission mediates aldosterone-induced podocyte injury and mitochondrial dysfunction. Am. J. Physiol.-Ren. Physiol 314, F798–F808 (2018).
16. Guo X, Sesaki H & Qi X Drp1 stabilizes p53 on the mitochondria to trigger necrosis under oxidative stress conditions in vitro and in vivo. Biochem. J 461, 137–146 (2014). [PubMed: 24758576]

17. Kornfeld OS et al. Interaction of mitochondrial fission factor with dynamin related protein 1 governs physiological mitochondrial function in vivo. Sci. Rep 8, 14034 (2018). [PubMed: 30232469]
18. Kornfeld OS et al. Mitochondrial Reactive Oxygen Species at the Heart of the Matter: New Therapeutic Approaches for Cardiovascular Diseases. Circ. Res 116, 1783–1799 (2015). [PubMed: 25999419]
19. Joshi AU et al. Inhibition of Drp1/Fis1 interaction slows progression of amyotrophic lateral sclerosis. EMBO Mol. Med 10, (2018).
20. Haileselassie B et al. Drp1/Fis1 interaction mediates mitochondrial dysfunction in septic cardiomyopathy. J. Mol. Cell. Cardiol 130, 160–169 (2019). [PubMed: 30981733]
21. Joshi AU, Ebert AE, Haileselassie B & Mochly-Rosen D Drp1/Fis1-mediated mitochondrial fragmentation leads to lysosomal dysfunction in cardiac models of Huntington's disease. J. Mol. Cell. Cardiol 127, 125–133 (2019). [PubMed: 30550751]
22. Haileselassie B et al. Myocardial oxidative stress correlates with left ventricular dysfunction on strain echocardiography in a rodent model of sepsis. Intensive Care Med. Exp 5, 21 (2017). [PubMed: 28405943]
23. Qvit N, Kornfeld OS & Mochly-Rosen D Engineered Substrate-Specific Delta PKC Antagonists to Enhance Cardiac Therapeutics. Angew. Chem. Int. Ed 55, 15672–15679 (2016).
24. Strom E et al. Small-molecule inhibitor of p53 binding to mitochondria protects mice from gamma radiation. Nat. Chem. Biol 2, 474–479 (2006). [PubMed: 16862141]
25. Huang C-Y et al. HMGB1 promotes ERK-mediated mitochondrial Drp1 phosphorylation for chemoresistance through RAGE in colorectal cancer. Cell Death Dis. 9, 1004 (2018). [PubMed: 30258050]
26. Shrum B et al. A robust scoring system to evaluate sepsis severity in an animal model. BMC Res. Notes 7, 233 (2014). [PubMed: 24725742]
27. O'Connell TD, Rodrigo MC & Simpson PC Isolation and culture of adult mouse cardiac myocytes. Methods Mol. Biol Clifton NJ 357, 271–296 (2007). [PubMed: 17172694]
28. Zhou Y-Y et al. Culture and adenoviral infection of adult mouse cardiac myocytes: methods for cellular genetic physiology. Am. J. Physiol.-Heart Circ. Physiol 279, H429–H436 (2000). [PubMed: 10899083]
29. Olsson MC, Palmer BM, Stauffer BL, Leinwand LA & Moore RL Morphological and Functional Alterations in Ventricular Myocytes From Male Transgenic Mice With Hypertrophic Cardiomyopathy. Circ. Res 94, 201–207 (2004). [PubMed: 14670849]
30. Duan J et al. Overexpression of alcohol dehydrogenase exacerbates ethanol-induced contractile defect in cardiac myocytes. Am. J. Physiol.-Heart Circ. Physiol 282, H1216–H1222 (2002). [PubMed: 11893554]
31. Silver RB Ratio Imaging: Measuring Intracellular Ca++ and pH in Living Cells. in Methods in Cell Biology vol. 72 369–387 (Elsevier, 2003). [PubMed: 14719341]
32. Nagata K et al. Early changes in excitation-contraction coupling: transition from compensated hypertrophy to failure in Dahl salt-sensitive rat myocytes. Cardiovasc. Res 37, 467–477 (1998). [PubMed: 9614501]
33. Dagda RK et al. Loss of PINK1 Function Promotes Mitophagy through Effects on Oxidative Stress and Mitochondrial Fission. J. Biol. Chem 284, 13843–13855 (2009). [PubMed: 19279012]
34. Guo X et al. Inhibition of mitochondrial fragmentation diminishes Huntington's disease–associated neurodegeneration. J. Clin. Invest 123, 5371–5388 (2013). [PubMed: 24231356]
35. Qi X, Qvit N, Su Y-C & Mochly-Rosen D Novel Drp1 inhibitor diminishes aberrant mitochondrial fission and neurotoxicity. J. Cell Sci jcs. 114439 (2012) doi:10.1242/jcs.114439.
36. Imbert N, Cognard C, Duport G, Guillou C & Raymond G Abnormal calcium homeostasis in Duchenne muscular dystrophy myotubes contracting in vitro. Cell Calcium 18, 177–186 (1995). [PubMed: 8529258]
37. Budd SL & Nicholls DG A Reevaluation of the Role of Mitochondria in Neuronal Ca2+ Homeostasis. J. Neurochem 66, 403–411 (2002).

38. Hartmann J & Verkhratsky A Relations between intracellular Ca $^{2+}$ stores and store-operated Ca $^{2+}$ entry in primary cultured human glioblastoma cells. J. Physiol 513, 411–424 (1998). [PubMed: 9806992]

39. Giorgi C, Marchi S & Pinton P The machineries, regulation and cellular functions of mitochondrial calcium. Nat. Rev. Mol Cell Biol 19, 713–730 (2018). [PubMed: 30143745]

40. Gao P, Yan Z & Zhu Z Mitochondria-Associated Endoplasmic Reticulum Membranes in Cardiovascular Diseases. Front. Cell Dev. Biol 8, 604240 (2020). [PubMed: 33240899]

41. Wang Y et al. Death-Associated Protein Kinase 1 Promotes Alveolar Epithelial Cell Apoptosis and Ventilator-Induced Lung Injury Through P53 Pathway. Shock 57, 140–150 (2022). [PubMed: 34265832]

42. Lomonosova E, Subramanian T & Chinnadurai G Mitochondrial localization of p53 during adenovirus infection and regulation of its activity by E1B-19K. Oncogene 24, 6796–6808 (2005). [PubMed: 16007153]

43. Joshi AU & Mochly-Rosen D Mortal engines: Mitochondrial bioenergetics and dysfunction in neurodegenerative diseases. Pharmacol. Res 138, 2–15 (2018). [PubMed: 30144530]

44. Landesberg G et al. Diastolic dysfunction and mortality in severe sepsis and septic shock. Eur. Heart J 33, 895–903 (2012). [PubMed: 21911341]

45. Hamilton S et al. Increased RyR2 activity is exacerbated by calcium leak-induced mitochondrial ROS. Basic Res. Cardiol 115, 38 (2020). [PubMed: 32444920]

46. Kubin A-M et al. Role of reactive oxygen species in the regulation of cardiac contractility. J. Mol. Cell. Cardiol 50, 884–893 (2011). [PubMed: 21320508]

47. Moris D et al. The role of reactive oxygen species in the pathophysiology of cardiovascular diseases and the clinical significance of myocardial redox. Ann. Transl. Med 5, 326–326 (2017). [PubMed: 28861423]

48. Wu X-Y, Luo A-Y, Zhou Y-R & Ren J-H N-acetylcysteine reduces oxidative stress, nuclear factor-κB activity and cardiomyocyte apoptosis in heart failure. Mol. Med. Rep 10, 615–624 (2014). [PubMed: 24889421]

Highlight:

- Mitochondrial localization of p53 after LPS treatment increases mitochondrial dysfunction and oxidative stress, leading to cardiomyocyte contractile dysfunction and murine mortality.
- Drp1 activation mediates p53 localization to the mitochondria via direct interaction between Drp1 and p53 in *in vitro* and murine sepsis models.
- ΨDrp1 peptide, an inhibitor of δPKC-dependent Drp1 phosphorylation and activation, decreases LPS-mediated Drp1/p53 interaction, prevents p53 localization to the mitochondria and mitochondrial dysfunction *in vitro* and in mice

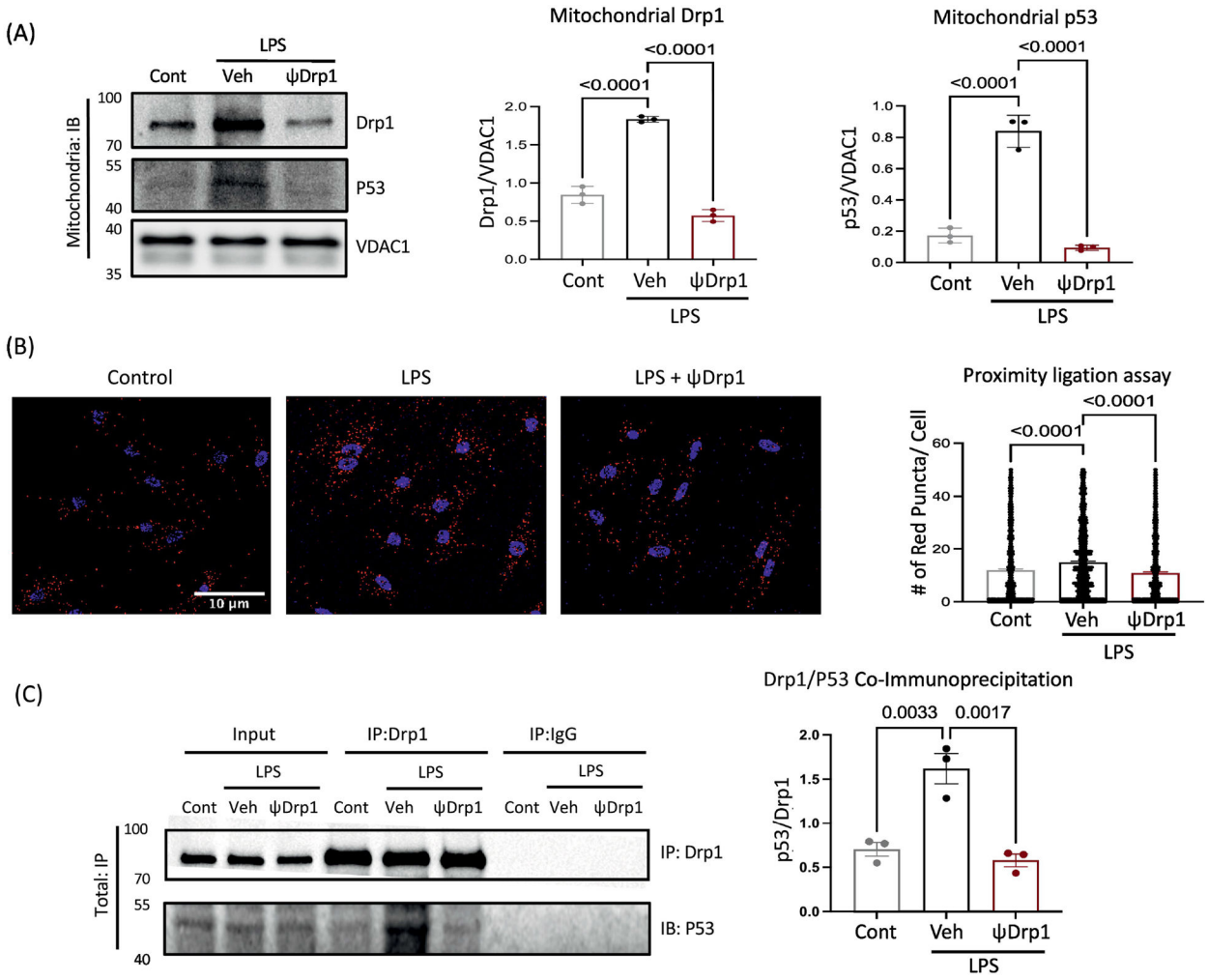

Figure 1. Mitochondrial localization of p53 is dependent on Drp1 activation and direct p53 and Drp1 interaction.

H9c2 cardiomyobasts were treated with LPS (1μg/ml), LPS+ΨDrp1(2μM). LPS induces mitochondrial localization of p53 and Drp1, demonstrated by increased content in mitochondrial enriched cell lysates, measured by western blot and quantified (n=3 biological replicates), that is inhibited by ΨDrp1 ($p < 0.001$) (A). Proximity ligation assay shows that under LPS stimulation, Drp1 binds to p53, and that inhibition of Drp1 activation with ΨDrp1 inhibits this interaction ($p < 0.001$) (single cell analysis of 784 cells per condition. All puncta from selected cells were included in analysis results represents n=3 biological replicates) (B). This physical interaction is further confirmed with immunoprecipitation with anti-Drp1 (representative images of n=3 biological replicates) ($p = 0.002$) (C). n represents independent experiments (biological replicate) each with a minimum of 3 technical replicates. Scale bar =10μm. Statistical analysis ANOVA with multiple comparison.

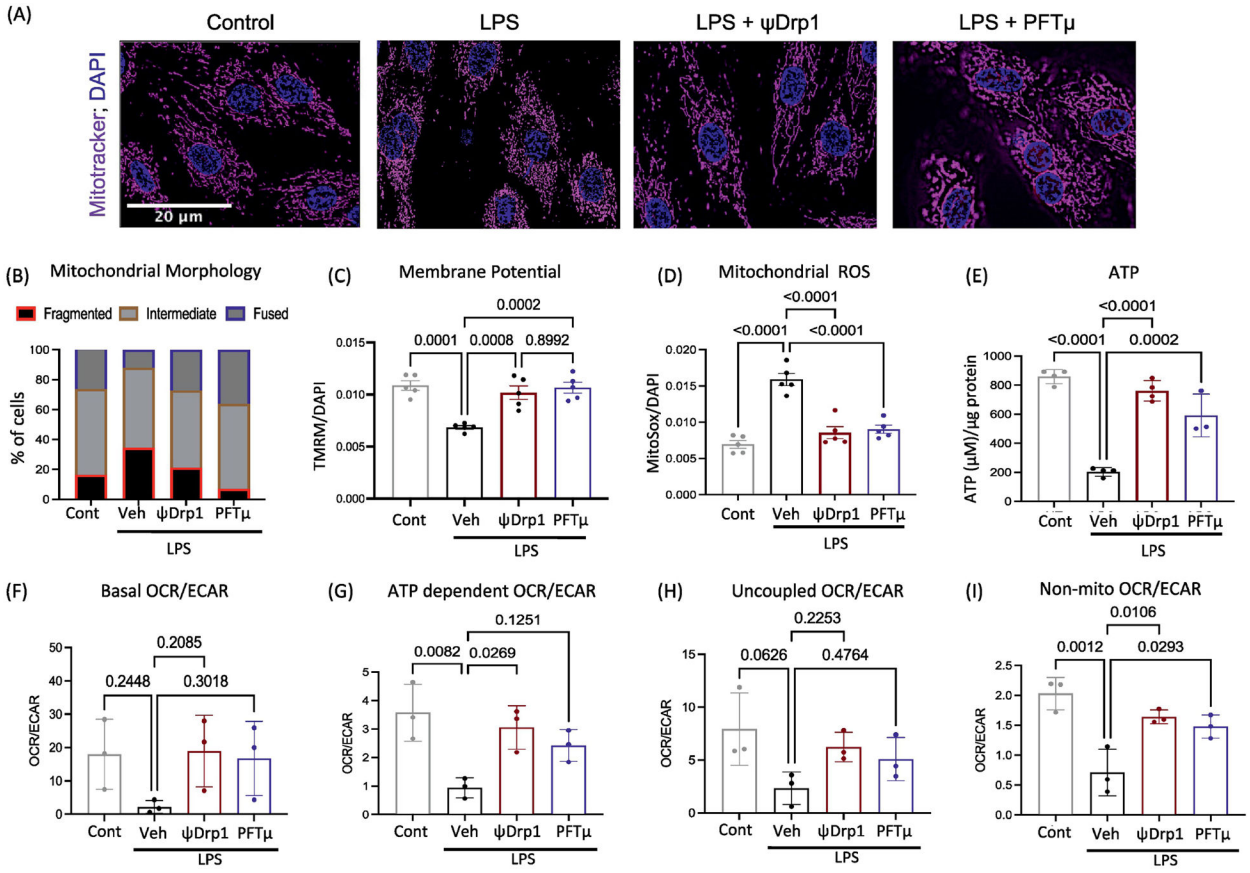

Figure 2. Inhibition of Drp1-p53 interaction and mitochondrial localization attenuates mitochondrial dysfunction in cell culture model of sepsis-induced cardiomyopathy.

Representative images of H9c2 cells stained with MitoTracker DeepRed (A) demonstrated increased percentage of cells with fragmented mitochondrial phenotype after treatment with LPS (1μg/ml), an effect that was attenuated with ΨDrp1 (2μM) ($p < 0.001$) and PFTμ (2.5μM) ($p < 0.001$) co-treatment (single cell analysis of n=3 biological replicates) (B). Inhibiting Drp1-p53 interaction and p53 mitochondrial localization blocked the LPS mediated mitochondrial damage, represented by membrane depolarization measured by TMRM (n=5 biological replicates) ($p < 0.001$) (C) and increase in oxidative stress as measured by MitoSox (n=5 biological replicates) ($p < 0.001$) (D), leading to increased ATP production (n=4 biological replicates) ($p < 0.001$) (E). LPS treatment of H9c2 cells resulted in a decrease in oxygen consumption rate (OCR)/extracellular acidification rate (ECAR) ratio, showing increased reliance on anaerobic metabolism (n=3 biological replicates) (F-I). Cotreatment with ΨDrp1 or PFTμ attenuated the LPS mediated metabolic shift represented by an increase in ATP-dependent (oligomycin) ($p = 0.02$) (G) and non-mitochondrial (rotenone/antimycin) (LPS vs LPS+ΨDrp1 ($p = 0.01$); LPS vs LPS+ PFTμ ($P = 0.03$)) (I) OCR/ECAR (n=3 biological replicates). n represents independent experiments (biological replicates) each with a minimum of 3 technical replicates. Scale bar = 20μm. Statistical analysis ANOVA with multiple comparison.

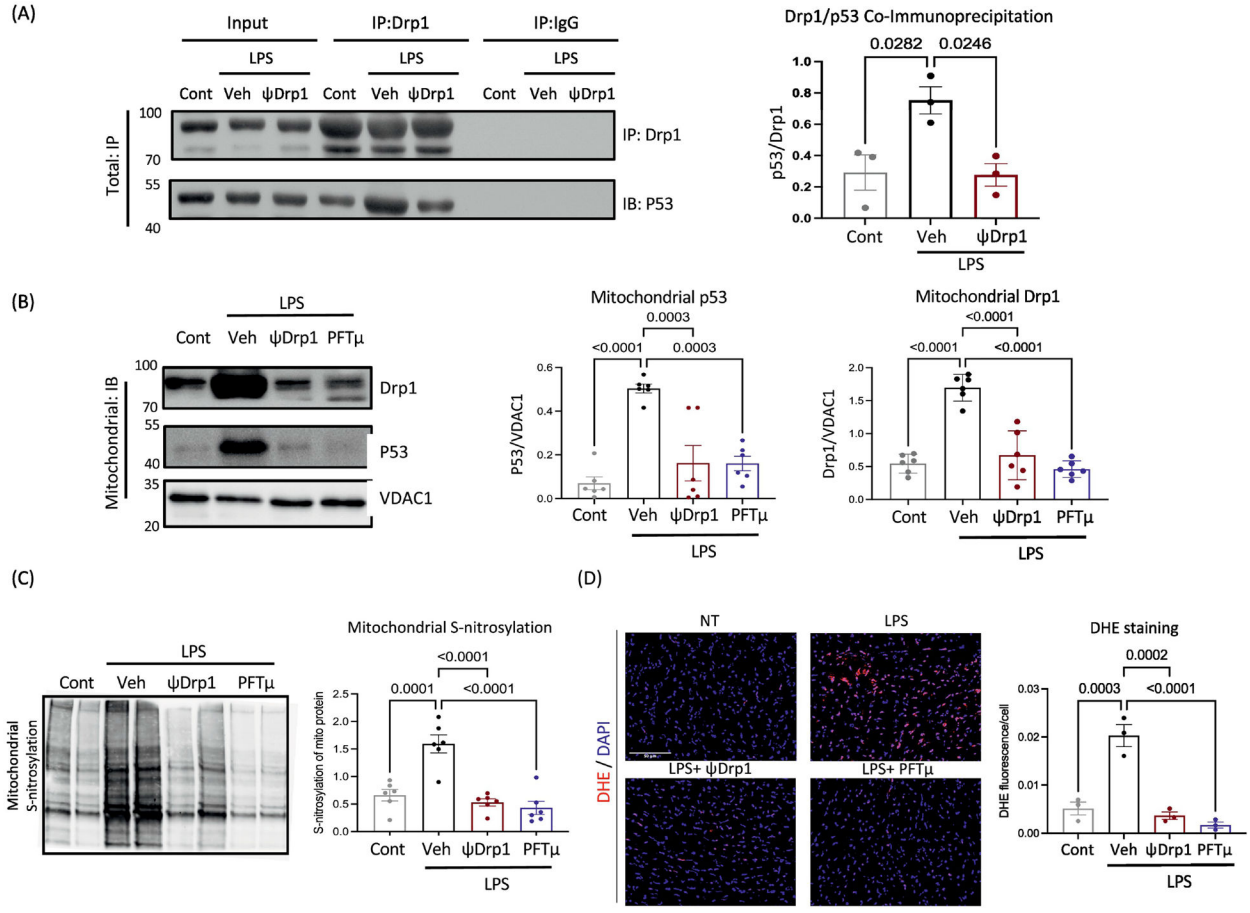

Figure 3. Pharmacologic inhibition of Drp1 activation or p53 mitochondrial localization limits cardiac oxidative stress in LPS murine model of sepsis.

BALB/c mice were treated with vehicle, LPS (8mg/kg), LPS + ΨDrp1(0.5mg/kg), or LPS + PFTμ (25mg/kg) and cardiomyocytes were isolated at 1 hour and 24 hour timepoints. LPS induced p53-Drp1 interaction ($p = 0.03$), measured by immunoprecipitation with anti-Drp1 (n=3 mice per condition) (A), as well as p53 mitochondrial localization ($p < 0.001$) (n=6 mice per condition) (B) within 1 hr, which is inhibited by both ΨDrp1 and PFTμ ($p < 0.001$). Decreasing mitochondrial localization of p53 using either PFTμ or ΨDrp1 attenuated LPS-mediated increase in oxidative stress in the mitochondria, as represented by oxidative post-translational modification S-nitrosylation ($p < 0.001$) (n=6 mice per condition) of mitochondrial lysate from heart tissue (C), as well as, in the overall cardiac tissue, as represented by dihydroethidium (DHE) staining at 24 hr. ($p < 0.001$) (n=3 mice per condition) (Figure 3D). n represents number of animals with a minimum of 3 technical replicates. Scale bar = 50–m. Statistical analysis ANOVA with multiple comparison.

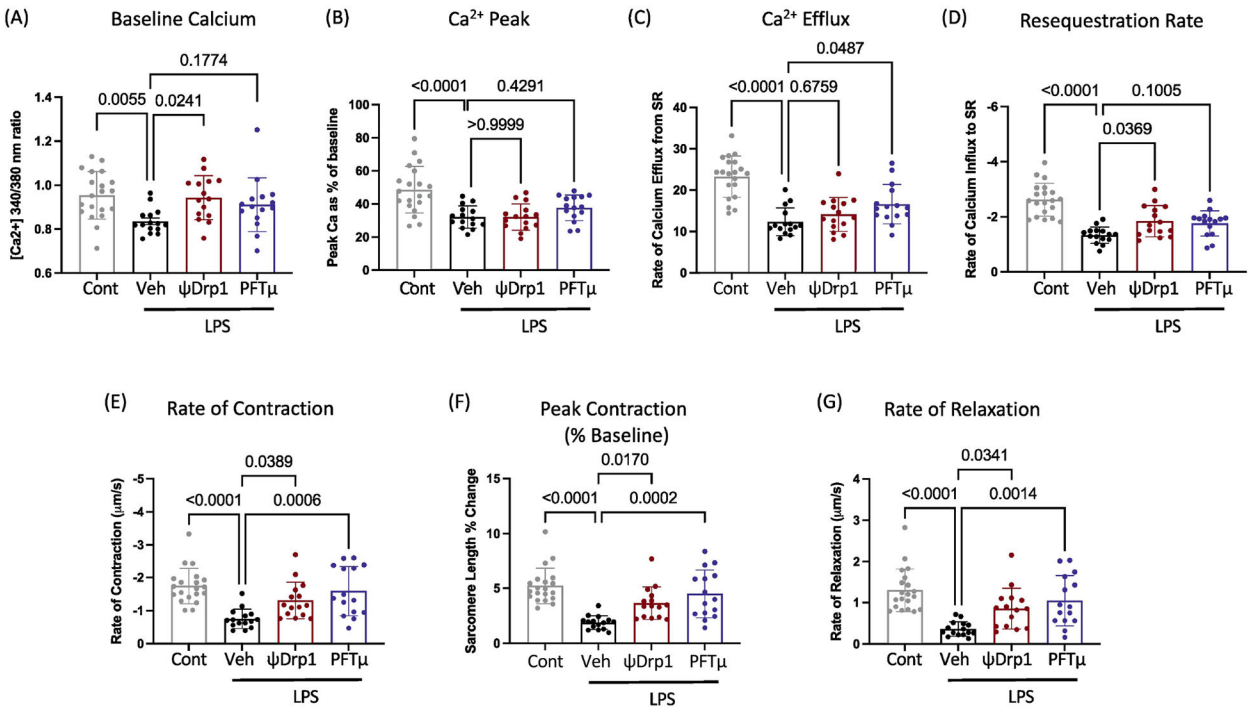

Figure 4. Pharmacological inhibition of Drp1 activation or p53 mitochondrial localization improves cardiomyocyte contractile function in LPS murine model of sepsis.

BALB/c mice were treated with vehicle (n=3 mice), LPS (13mg/kg) (n=4 mice), LPS + ΨDrp1(0.5mg/kg) (n=4 mice), or LPS + PFTμ (25mg/kg) (n=4 mice) and cardiomyocytes were isolated at 24 hrs for evaluation of calcium flux and contractile force. Isolated cardiomyocytes from LPS treated animals had a significant decrease in calcium flux at baseline ($p=0.005$) (A) and following stimulation represented by decrease in peak calcium ($p < 0.001$) (B), calcium efflux ($p < 0.001$) (C) and resequestration rate ($p < 0.001$) (D). Co-treatment with ΨDrp1 restored baseline calcium and resequestration rate ($p=0.04$) while co-treatment with PFTμ improved calcium efflux ($p=0.05$). When evaluating contractility, LPS treatment decreased rate of contraction ($p < 0.001$) (E), peak sarcomere length ($p < 0.001$) (F) as well as rate of relaxation ($p < 0.001$) (G). Both ΨDrp1 and PFTμ reversed LPS mediated derangements in contractility (E-G). n represents independent experiments with each data point representing results from single cell. Statistical analysis ANOVA with multiple comparison.

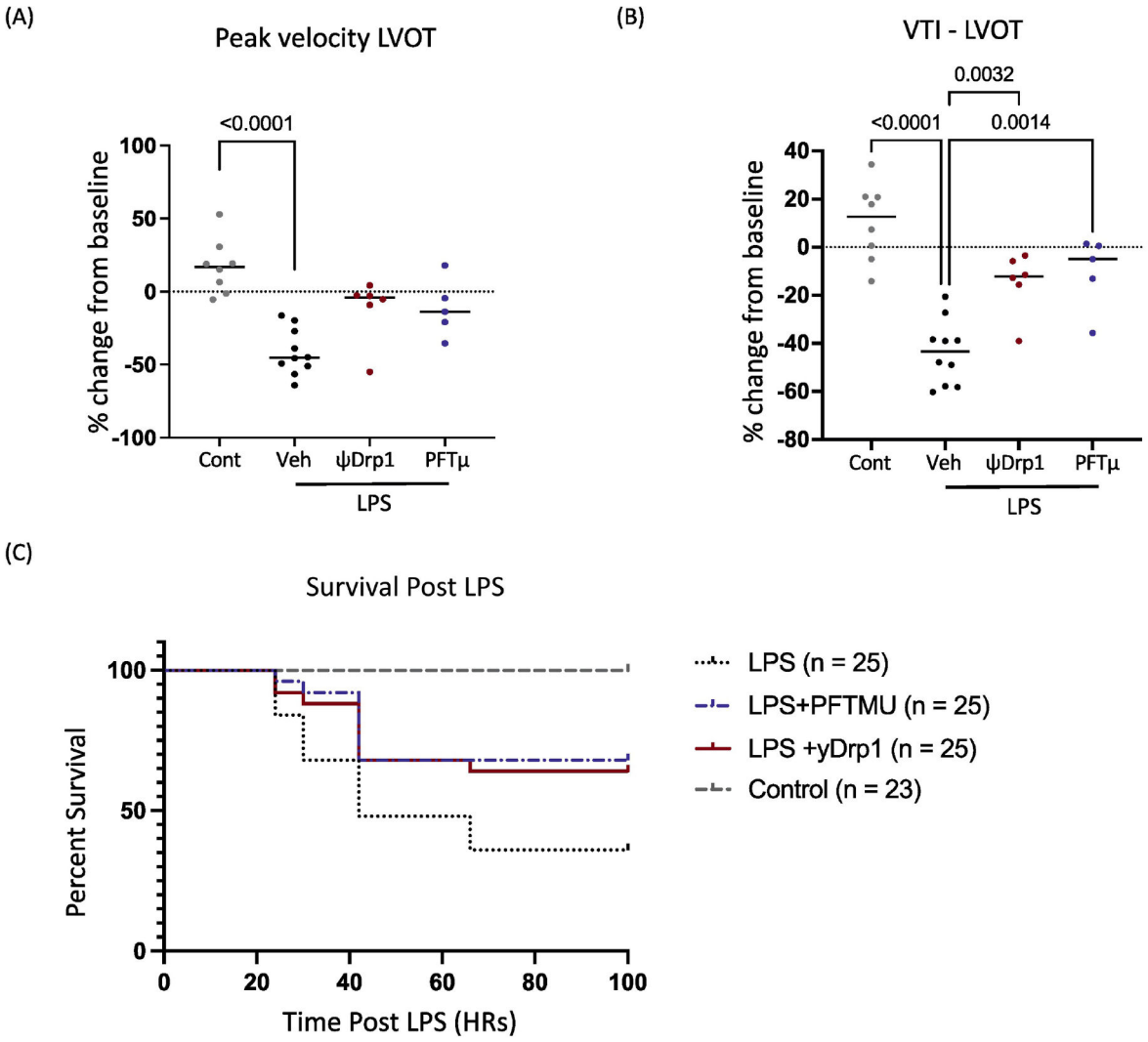

Figure 5. Inhibition of Drp1/p53 interaction improves cardiac function and decreases mortality in LPS murine model of sepsis.

BALB/c mice underwent echocardiogram at baseline and at 18 hours following treatment with vehicle (n=8 mice), LPS (n=10 mice), LPS + ΨDrp1(n=6 mice), or LPS + PFTμ (n=6 mice). Pulse wave doppler was used to attain maximum velocity and velocity time integral (VTI) across the left ventricular outflow tract. Treatment with ΨDrp1 and PFTμ both partially rescued LPS mediated decrease in maximum velocity (A) and VTI (B) ($p < 0.001$) BALB/c mice were treated with vehicle (n=23 mice), LPS (13mg/kg) (n=25 mice), LPS + ΨDrp1(0.5mg/kg) (n=25 mice), or LPS + PFTμ (25mg/kg) (n=25 mice) and evaluated for illness severity and mortality. LPS-treated mice had a significant increase in mortality [cont (veh) = 0% vs LPS + veh = 64%; $p<0.0001$] which was decreased with ΨDrp1 [LPS+ veh = 64% vs LPS+ ΨDrp1= 40%; $p=0.044$] and PFTμ treatment [LPS+ veh = 64% vs LPS+ PFTμ = 32%; $p=0.023$] (C). n = individual animals results are a pooled from 3 independent experiments. Statistical analysis ANOVA with multiple comparison and log-rank test for comparison of survival curves.